Biosorption performance evaluation of heavy metal onto aerobic granular sludge-derived biochar in the presence of effluent organic matter via batch and fluorescence approaches

Dong Wei [a], Huu Hao Ngo [b], Wenshan Guo [b], Weiying Xu [a], Bin Du [a]*, Malik Saddam Khan [c], Qin Wei [c]

[a] *School of Resources and Environment, University of Jinan, Jinan 250022, PR China*

[b] *School of Civil and Environmental Engineering, University of Technology Sydney, Broadway, NSW 2007, Australia*

[c] *Key Laboratory of Chemical Sensing & Analysis in Universities of Shandong, School of Chemistry and Chemical Engineering, University of Jinan, Jinan 250022, PR China*

Abstract

In present study, the biosorption process of Cu(II) onto aerobic granular sludge-derived biochar was evaluated in the absence and presence of effluent organic matter (EfOM) by using batch and fluorescence approaches. It was found that EfOM gave rise to enhancement of Cu(II) removal efficiency onto biochar, and the sorption data were better fitted with pseudo-second order model and Freundlich equation, in despite of the absence and presence of EfOM. According to excitation-emission matrix (EEM), EfOM was mainly comprised by humic-like substances and fulvic-like substances and their intensities were reduced in the addition of biochar and Cu(II) from batch biosorption process. Synchronous fluorescence spectra coupled to two-dimensional correlation spectroscopy (2D-COS) further implied that a successive fluorescence quenching was observed in various EfOM fractions with the increasing Cu(II) concentration. Moreover, fulvic-like fraction was more susceptibility than other

* Corresponding author. Tel: +86 531 8276 7370; fax: +86 531 8276 7370.
E-mail address: dubin61@gmail.com (B. Du)

fractions for fluorescence quenching of EfOM.

Keywords: Biorption; Effluent organic matter (EfOM); Biochar; Excitation-emission matrix (EEM); Heavy metal.

1. Introduction

With the rapid development of the economy, a great number of industries, such as metallurgy, machinery manufacturing, chemical, electronics, textile, instrument and printing etc., produce and discharge hazardous wastes based various heavy metals into the environment. The increasing heavy metal pollution has become one of the most worldwide environmental problems facing humanity, which brings about serious water pollution, threatens human health and ecosystem (Wang and Chen, 2009). Due to their non-degradable, accumulation and persistent characteristics, the removal and elimination of toxic metal ions from contaminated water is significant necessary prior to discharge into receiving water.

Till now, numerous methods have been proposed for efficient heavy metal removal from aqueous solution, including chemical precipitation, ion exchange, adsorption, membrane filtration and electrochemical technologies etc. (Fang et al., 2017; Ming et al., 2012). Among all above these techniques, adsorption is regarded as one of the most important physico-chemical treatment processes due to its advantages of high efficiency, simplicity of design and ease of operation (Cui et al., 2015; Fomina and Gadd, 2014; He and Chen, 2014). As one kind of carbon-enriched biosorbents, biochar has been recently attracted considerable attention and successfully applied for treating various heavy metals because of its low-cost, resource abundant, eco-friendly,

and mechanical and thermal stability (Tavakoli et al., 2017). At present, a wide range of biological raw materials (e.g. bacteria, sludge, biomass, algae and fungi etc.), either in original or modified forms, have been developed as precursors for preparing biochar and subsequent heavy metal sorption (Devi and Saroha, 2014; Inyang et al., 2016). Tong et al. (2011) prepared biochar from three crop straws as metal-removal adsorbents, suggesting that biochar had great adsorption capacity to remove Cu(II) from aqueous solution. Kołodyńska et al. (2017) compared the sorption performance of Cu(II), Zn(II), Cd(II), Co(II) and Pb(II) by using commercial activated carbon and biochar, suggesting that heavy metal ions were removed more efficiently through biochar than activated carbon.

The sorption property of heavy metal onto biochar is influenced by many operational factors, such as initial metal concentration, contact time, temperature and pH value etc. (Inyang et al., 2016; Qian et al., 2016). As a well-known heterogeneous mixture of complex organic compounds, effluent organic matter (EfOM) is ubiquitous in the environment originating from biologically treated wastewater with the main fractions of humic acid (HA) and fulvic acid (FA) (Vigneswaran, 2006). It is generally accepted that HA and FA are chemically heterogeneous compounds that can interact with the surface of biosorbents, alter their physicochemical properties, and therefore influence their sorption behaviors (Yang and Xing, 2009). Moreover, a variety of functional groups are present in EfOM at different proportions and configurations, such as carbonyl, carboxyl, aromatic, acetal, and phenolic groups etc., which could also allow them to complex with heavy metal ions (Tian et al., 2012). Although the

presence of HA or FA on the influence of metal sorption performance has already been acknowledged in recent literatures, there is still lack of information regarding to the effect of EfOM on metal sorption by using biochar. Especially, both FA and HA coexisted in EfOM have various binding sites that could compete with the target heavy metal during sorption process, which would be much more complicated than that of single system containing only FA or HA. Therefore, it is of great significance to investigate the adsorption behavior of heavy metal onto biochar in the presence of EfOM.

Hence, the objective of this study was to evaluate the presence of EfOM on the influence of metal sorption onto biochar via batch and spectral approaches. To achieve this purpose, biochar was prepared by using aerobic granular sludge (AGS) as raw material. Cu(II) was selected as the target metal ion for evaluating the sorption performance and difference in the presence and absence of EfOM. Moreover, the interaction between EfOM and Cu(II) in the sorption process was evaluated by using a combined use of 3D-EEM, fluorescence regional integration (FRI), synchronous fluorescence and two-dimensional correlation spectroscopy (2D-COS). The obtained results could provide an insightful understanding of metal bisorption in the presence of EfOM by application of fluorescence spectroscopy.

2. Materials and methods

2.1 Effluent organic matter

The raw EfOM sample was collected before the disinfection step at the

secondary settling tank in a municipal wastewater treatment plant (WWTP) located at Jinan, China. The WWTP used a combined anaerobic/anoxic/aerobic activated sludge process with a treatment capacity of 50,000 m^3/day. Prior to experiment, the EfOM sample was filtered through a 0.45 nm filter to remove particles and then stored in the refrigerator at 4 ^oC before use. The total organic carbon (TOC) of the EfOM sample was typically around 9.0 mg/L.

2.2 Preparing of AGS-BC

Aerobic granular sludge (AGS) was used as raw material for biochar preparation, which was collected from our lab-scale SBR at the end of aeration process. The detailed synthetic wastewater of SBR could be found elsewhere (Wei et al., 2014). Previous literature has been proved that AGS based biochar has a better sorption capacity than that of activated sludge (Liu et al., 2016). The raw AGS for carbonization had a regular and round-shaped outer structure with an average size of about 2 mm. All the sludge samples were washed three times by using deionized water to remove the surface soluble ions.

AGS-BC was prepared by using a chemical activation method according to the literature reported by Tay et al. (2001). The raw sludge sample was firstly dried at 105 ^oC for 24 h to achieve constant weight. Next, 10 g of samples were added into 25 mL of 5 mol/L $ZnCl_2$ solution for 24 h at temperature. After that, the sample was carbonized at 650 ^oC for 2h in a quartz tube under N_2 atmosphere. After cooling down to room temperature, the obtained products were wished with 3M HCl, followed by filtration and dried at 105 ^oC.

2.3 Experimental design

For comparing the effect of EfOM on the metal bisorption performance, batch sorption tests were carried out in 50-mL conical flasks at 25 ^{o}C, in which Cu(II) and EfOM were added and pre-equilibrated for 24 h before AGS-BC was added. More detailed, sorption kinetic experiment was determined by analyzing adsorptive uptake of 20 mL Cu(II) at 20 mg/L onto 20 mg AGS-BC from its aqueous solution at different time intervals in the range of 0-360 min. The initial pH value of the mixed solution was adjusted to 5.0 by using 0.1 mol/L to avoid of precipitation, as similarly reported by Sun et al. (2009). The sorption isotherm was carried out with initial Cu(II) concentrations varied from 5 to 80 mg/L sorption onto 20 mg AGS-BC at pH 5.0 for 48 h to ensure equilibrium.

2.4 Fluorescence analysis

3D-EEM spectra were scanned with a luminescence spectrometer (LS-55, Perkin-Elmer Co., USA). Detailed, EEM scans were made at the emission wavelengths (Em) from 280 to 550 nm with a 0.5 nm-increment and at the excitation wavelengths (Ex) from 220 nm to 400 nm with a 10 nm-step. The excitation and emission slits were both 10 nm. The scanning speed was set at 1200 nm/min for all the fluorescence measurements.

FRI method was also applied to quantitatively determine the configuration and heterogeneity of EfOM in EEM spectra. EEM spectra were divided into five consecutive regions (aromatic protein I, aromatic protein II, fulvic acid-like, soluble

microbial by product-like, and humic acid-like for Region I-V, respectively), corresponding to excitation/emission (Ex/Em) wavelength ranges of 220-250/280-330 nm, 220-250/330-380 nm, 220-250/380-550 nm, 250-400/280-380 nm, and 250-400/380-550 nm, respectively. Detailed information about the analysis of FRI technique could be found elsewhere (Chen et al., 2003).

The interaction between EfOM and Cu(II) was investigated by using fluorescence quenching titration experiment. EfOM exhibits fluorescence that is quenched upon binding to Cu(II). More detailed, 5 mL of EfOM solution was added with a series volume of pre-determined Cu(II) solution (100 mg/L) in a 10 mL volumetric flask at pH 5.0. The final Cu(II) concentrations in mixed solution were successively varied from 0 to 50 mg/L. Afterwards, the mixed solution was with oscillator for 12 h to ensure equilibrium before spectra measurement. A set of dosage-dependent fluorescence spectra were recorded through synchronous fluorescence spectra by simultaneous scanning the excitation and emission wavelength in the range of 250 to 550 nm with a constant offset ($\Delta\lambda$) of 60 nm.

2.5 Analytical methods

The specific surface area and pore structure parameters of AGS-BC were determined by using Micromeritics ASAP 2020 surface area and porosity analyzer (Quantachrome, United States). Fourier Transform infrared spectroscopy (FTIR) in the spectral range of 4000-400 cm^{-1} was measured by using a Perkin-Elmer Spectrum One spectrometer (United States). The surface physical morphology of biochar was observed by using a scanning electron microscope (SEM, Quanta 250 FEG). The

surface charge of the samples was determined by measuring the zeta potential by using a Malvern Zetameter (Zetasizer 2000). The adsorption experimental results of Cu(II) were analyzed in triplicate, and the averaged data were presented here. The synchronous and the asynchronous maps in 2D-COS for extending the spectra along the second dimension could be obtained from the method reported by Noda and Ozaki (2005).

3. Results and discussion

3.1 Characterization of AGS-BC

The physical and chemical characteristics of prepared AGS-BC were observed by using BET, FTIR spectra, SEM and Zeta potential. It was found that BJH desorption cumulative volume of pores and BET surface area of biochar were 0.6985 cm^3/g and 1175.1 m^2/g, respectively. The surface area of AGS-BC was much higher than the previous literature reported by using activated sludge as raw material (Al-Malack and Dauda, 2017), which is beneficial for surface sorption. The main functional groups in AGS-BC included -OH at 3436 cm^{-1}, C=O at 1631 cm^{-1} and C-O-C at 1212 cm^{-1}. It was found from SEM that different pores and cavities were observed in the surface of biochar, which might be resulted from the decomposition of $ZnCl_2$ during the thermal treatment process. Zeta potential of biochar decreased from 11.6 to -4.7 mV in the pH range of 2-10, respectively. The negative Zeta potential (pH>5.0) of the sludge-based biochar implied that the positively charged metal pollutants may be more easily adsorbed.

3.2 Effect of contact time on Cu(II) sorption

The effect of contact time on Cu(II) sorption onto AGS-BC was evaluated in the absence and presence of EfOM. It is clearly observed that Cu(II) sorption onto AGS-BC occurred in two steps as a function of contact time: a very rapid initial sorption, followed by a long period of much slower uptake, as similarly reported by Wei et al. (2016c). Cu(II) sorption rate was much higher in the beginning due to larger surface area available of adsorbent, in spite of the presence and absence of EfOM. However, Cu(II) sorption onto AGS-BC achieving equilibrium were at 60 and 300 min in the presence and absence of EfOM, respectively. The presence of EfOM gave rise to enhancement of Cu(II) removal, whose removal increased almost from 57.4% to 76.8%. The result suggested that the addition of EfOM increased the sorption property of Cu(II) onto AGS-BC.

In order to elucidate the potential rate-limiting steps of biosorption, the batch results of Cu(II) onto AGS-BC in the presence and absence of EfOM were analyzed according to pseudo-first-order and pseudo-second-order models. The above two kinetic models can be expressed as follows (Eqs (1-2)):

$$\ln(q_e - q_t) = \ln q_e - k_1 t \quad (1)$$

$$\frac{t}{q_t} = \frac{1}{k_2 q_e^{\,2}} + \frac{1}{q_e} t \quad (2)$$

Where q_e (mg/g) is the adsorbed amount at time t, q_t (mg/g) is the adsorbed amount at equilibrium, k_1 (1/min) is the rate constant of pseudo-first-order kinetic model, and k_2 (mg/ (g min)) are the equilibrium rate constant of the

pseudo-second-order kinetic model.

Fig.1 shows the pseudo-first-order and pseudo-second-order kinetics fit of Cu(II) sorption onto AGS-BC in the absence and presence of EfOM. Table 1 summarizes the constants and correlation coefficients for the kinetic models. It was observed that pseudo-second order kinetic equations had higher R^2 values (0.9965 and 0.9999) in despite of the absence or presence of EfOM, suggesting that it could be taken as the better fit equations for the description of the mechanism of sorption of Cu(II) ion. The result indicated that chemical adsorption rather than physical adsorption contributes mainly to the adsorption of Cu(II) onto sludge-based biochar. Cui et al. (2016) also investigated the Cd(II) sorption onto different wetland-plant derived biochars, suggesting that sorption kinetic data were better fitted to pseudo-second-order model than the pseudo-second-order and the intra-particle diffusion models.

3.3 Adsorption isotherm

The adsorption isotherm could provide the detailed information about the surface properties of adsorbent, the adsorption behavior and the design of adsorption systems (Fu et al., 2015). For better predicting the isotherm results, two common models including Langmuir and Freundlich are described based on the adsorption equilibrium data. Langmuir and Freundlich models can be described in linear form as follows:

$$q_e = \frac{bq_m c_e}{1 + bc_e} \tag{3}$$

$$q_e = K_f c_e^{1/n} \tag{4}$$

Where c_e (mg/L) is the equilibrium concentration of Cu(II), q_e (mg/g) is the adsorption capacity, q_m (mg/g) is the theoretical maximum sorption capacity, b (L/mg) is the Langmuir constant related to adsorption energy, K_f is the binding energy constant reflecting affinity of adsorbents to Cu(II), and n is the Freundlich constant.

Fig. 2 shows the non-liner Langmuir and Freundlich adsorption isotherms fit of Cu(II) sorption onto AGS-BC in the presence and absence of EfOM. Table 2 summarizes the constants and correlation coefficients of adsorption isotherms for the sorption of Cu(II) onto AGS-BC with and without EfOM. It was found that Cu(II) sorption onto biochar in the presence of EfOM was significantly higher than in the absence system. The R^2 values of the Freundlich model were higher than those of the Langmuir model, indicating that the Freundlich model fitted the adsorption data better than the Langmuir model. According to Langmuir isotherm model, the calculated maximum adsorption capacity (q_m) are of 18.5 and 20.0 mg/g for AGS-BC in the absence and presence of EfOM, respectively, suggesting that EfOM played an positive effect for treating Cu(II) in the biosorption process. Freundlich isotherm model can be used to describe the sorption on heterogeneous surfaces as well as a multilayer sorption. It assumes that the uptake of adsorbate ions occurs on a heterogeneous adsorbent surface (Ewecharoen et al., 2008). Similar observation has been reported by Pellera et al. (2012), who found that the equilibrium of Cu(II) sorption onto biochar prepared from agricultural by-products was better fitted by Freundlich isotherm. In present study, the values of $0.1<1/n<1.0$ in Freundlich model implied that adsorption of Cu(II) onto biochar are favorable. Moreover, the K_f values

obtained from the Freundlich model were 2.919 and 5.238 in the absence and presence of EfOM, respectively. The result suggested that the presence of EfOM enhanced the metal binding affinity.

Till now, the effect of FA or FA on the sorption performance has been well reported in previous studies with positive or negative roles. Sheng et al. (2010) proved that a positive effect of HA/FA on Cu(II) adsorption onto multiwalled carbon nanotubes (MWCNTs) was found at pH<7.5, that was consistent with our observation of Cu(II) sorption onto biochar. Similar observation has also been reported by Sun et al. (2012), who reported that Cu(II) adsorption by MWCNTs increased with increasing natural organic matter (NOM) concentration. In contrast, Yu et al. (2012b) found that the presence of EfOM significantly reduced the adsorption capacities and sorption rates of perfluorinated compounds onto activated carbon.

3.4 Fluorescence characterization of EfOM in the sorption of Cu(II) onto AGS-BC

3.4.1 3D-EEM

It is well reported that the interaction between HA or FA and sorbent not only alter the surface properties and environmental behavior of these sorbent materials, but also affect the adsorption of coexisting contaminants (Tian et al., 2012). Therefore, 3D-EEM was used to better understand the changes in chemical components of EfOM in batch biosorption process of Cu(II) onto AGS-BC. It was found from Fig. 3A that two main fluorescence peaks were observed in the raw EfOM sample. Peak A and Peak B were located at Ex/Em of 330/414 and 250/423 nm, respectively, which were represented as humic-like substances and fulvic -like substances (Wei et al., 2016a).

The presence of humic-like substances may be related to a biological production and activity of microorganisms, which could be referred to the non-biodegradable component in EfOM samples (Wei et al., 2016c). Compared to previous literature (Phong and Hur, 2016), Peak C at Ex/Em of about 250/350 nm was assigned to protein-like substances, whose fluorescence intensity was much lower than those of humic-like substances and fulvic -like substances. The reason may be attributed that protein-like substances were representative of the biodegradable EfOM and therefore could be utilized by activated microorganism (Yang et al., 2017).

The intensities of Peak A and Peak B in raw EfOM were 499.9 and 471.8 a.u., respectively. Peak A were generally reduced to 426.7, 56.1 and 29.2 a.u. in the presence of AGS-BC, Cu(II) and AGS-BC+Cu(II), whereas those in Peak B were reduced to 315.8, 61.6 and 44.1 a.u., respectively. Data implied that the intensities of both peaks were significantly reduced in the presence of Cu(II) and AGS-BC. The result strongly proved that HA and FA in EfOM could react with both AGS-BC and Cu(II) during the biosorption process. Their interaction may be the possible reason for the changed sorption performance of Cu(II) onto biochar. More detailed, EfOM could adsorb onto the surfaces of the AGS-BC and may introduce more binding sites and negative charges to AGS-BC surface, increasing the adsorption of Cu(II) through chemical complexation and electrostatic attraction, as similarly reported by Sun et al. (2012) and Yang et al. (2014).

3.4.2 FRI analysis

Fig. 4 shows the FRI distribution of EfOM samples during the biosorption

process. In the raw EfOM (sample A in Fig. 4), Region III (fulvic acid-like substances) and Region V (humic acid-like organics) expressed significant higher percentages (27.8% and 34.7%) than those of other Regions, suggesting that they had the relatively high amounts in EfOM. The FRI observation was consistent with the Peak A and Peak B fluorescence intensities in 3D-EEM (Fig. 3A). It was found that the percentages of Region III and Region V were reduced relatively higher degrees after interaction with single Cu(II) and AGS-BC, whose values were changed to 24.8% and 24.4%, respectively. Therefore, the coexisted fulvic-like and humic-like substances in EfOM may be referred to react with the adsorbate and adsorbent. Additionally, there was a highest reduced percentage of Region V in the presence of both Cu(II) and AGS-BC, whose value was accounted for 18.2 % of the total fluorescence percentages, suggesting that humic-like substances played significant role in metal sorption process. Xu et al. (2016) also indentified the changes in different regions percentages during the interactions between metal oxide nanoparticles and extracellular polymeric substances (EPS) by using EEM-FRI.

3.4.3 Synchronous fluorescence spectra

Since both FA and HA in EfOM containing different types of functional groups could react with Cu(II), therefore, the interaction between FA/HA and Cu(II) was important and complex than the single system. In present study, synchronous fluorescence spectra were further applied for better understand the interaction between EfOM and Cu(II), as displayed in Fig. 5. The whole wavelength of 250-300, 300-380 and 380-550 nm could be assigned to protein-like, fulvic-like, and

humic-like fluorescence fractions (Hur et al., 2011). It was found from Fig.5 that a successive fluorescence quenching was observed with the increasing Cu(II) concentration from 0 to 50 mg/L, suggesting that the fluorophore-related functional groups in EfOM was influenced by the presence of heavy metal. A much higher fluorescence peak was observed at 342.5 nm in the raw EfOM, suggesting that fulvic-like fraction was the main component in EfOM that was consistent with the result of EEM. Data implied that the intensity of fulvic-like fraction was significantly reduced from 683.6 to 237.9 a.u. after binding to 50 mg/L Cu(II),which expressed much higher degree than other components in EfOM. Chen et al. (2015) also researched the binding characteristics of Cu(II) onto dissolved organic matter by using synchronous fluorescence spectra, suggesting that an increase in Cu(II) concentration caused a higher extent of fluorescence quenching for all the fractions, which was similar to our observation.

3.4.4 2D-COS

To provide more information on the heterogeneous distribution of metal binding sites within EfOM, 2D-COS was applied to synchronous fluorescence spectra of EfOM with Cu(II) addition as the external perturbation. Two types of the maps, synchronous 2D and asynchronous 2D spectra, were generated from 2D-COS (Wei et al., 2016b). As shown in Fig. 6A, one positive autopeak (345 nm) was indentified along the diagonal line of the synchronous map, indicating that the spectral changes proceed in the same direction for the corresponding areas. Moreover, fulvic-like fraction was more susceptibility than thoses of other fractions in EfOM (e.g.

protein-like and humic-like fractions).

Asynchronous map reveals a sequential or successive change in the spectral intensities in response to external perturbation (Yu et al., 2012a). As shown in Fig. 6b, one obvious negative area (250-300, 300-400 nm) was observed. According to Noda' rule, EfOM fluorescence quenching took place in the order of 300-400 nm >250-300 nm. Therefore, it could be concluded from asynchronous map that, for EfOM quenching, fulvic-like fraction and the short wavelength of humic-like fraction took place earlier than other fluorescence components.

4. Conclusions

In summary, the influence of EfOM sorption onto sludge-based biocher was evaluated by using batch and fluorescence approaches. For sorption process, Cu(II) sorption onto biochar followed pseudo-second order kinetic model and Freundlich model in both absence and presence of EfOM. Spectroscopic observation implied that FA and HA were two main components in EfOM and expressed decreased trends in the addition of Cu(II), which may be the reason for enhanced biosorption performance. The result of present study is helpful to provide insightful information on the meal treatment process by using biochar.

5. Acknowledgements

This study was supported by Natural Science Foundation of Shan dong Province (ZR201702070162), the Natural Science Foundation of Chinese Province (21377046), Special project of independent innovation and achievements transformation of

Shandong Province (2014ZZCX05101), Science and technology development plan project of Shandong province (2014GGH217006), and QW thanks the Special Foundation for Taishan Scholar Professorship of Shandong Province and UJN (No.ts20130937).

References

[1] Al-Malack, M.H., Dauda, M. 2017. Competitive adsorption of cadmium and phenol on activated carbon produced from municipal sludge. J Environ Chem Eng. 5, 2718-2729

[2] Chen, W., Habibul. N., Liu. X.Y., Sheng, G.P., Yu, H.Q., 2015. FTIR and synchronous fluorescence heterospectral two-dimensional correlation analyses on the binding characteristics of copper onto dissolved organic matter. Environ. Sci. Technol. 49, 2052-2058.

[3] Chen, W., Westerhoff, P., Leenheer, J.A., Booksh, K., 2003. Fluorescence excitation-emission matrix regional integration to quantify spectra for dissolved organic matter. Environ. Sci. Technol. 37, 5701-5710.

[4] Cui, L., Guo, X., Qin, W., Wang, Y., Liang, G., Yan, L., Tao, Y., Du, B. 2015. Removal of mercury and methylene blue from aqueous solution by xanthate functionalized magnetic graphene oxide: Sorption kinetic and uptake mechanism. J. Colloid Interface Sci. 439, 112-120.

[5] Cui, X., Hao, H., Zhang, C., He, Z., Yang, X. 2016. Capacity and mechanisms of ammonium and cadmium sorption on different wetland-plant derived biochars. Sci. Total Environ. 539, 566-575.

[4] Devi, P., Saroha, A.K. 2014. Risk analysis of pyrolyzed biochar made from paper mill effluent treatment plant sludge for bioavailability and eco-toxicity of heavy metals. Bioresour. Technol. 162, 308-315.

[5] Fang, X., Li, J., Li, X., Pan. S., Zhang, X., Sun. X., Shen. J., Han. W., Wang, L. 2017. Internal pore decoration with polydopamine nanoparticle on polymeric ultrafiltration membrane for enhanced heavy metal removal. Chem. Eng. J. 314, 38-49.

[6] Fomina, M., Gadd, G.M. 2014. Biosorption: current perspectives on concept, definition and application. Bioresour. Technol. 160, 3-14.

[7] Fu, J., Chen, Z., Wang, M., Liu, S., Zhang, J., Zhang, J., Han, R., Xu, Q. 2015. Adsorption of methylene blue by a high-efficiency adsorbent (polydopamine microspheres): Kinetics, isotherm, thermodynamics and mechanism analysis. Chem. Eng. J. 259, 53-61.

[8] He, J., Chen, J.P. 2014. A comprehensive review on biosorption of heavy metals by algal biomass: materials, performances, chemistry, and modeling simulation tools. Bioresour. Technol. 160, 67-78.

[9] Hur, J., Jung, K.Y., Jung, Y.M. 2011. Characterization of spectral responses of humic substances upon UV irradiation using two-dimensional correlation spectroscopy. Water Res. 45, 2965-2974.

[10] Inyang, M.I., Gao, B., Yao, Y., Xue, Y., Zimmerman, A., Mosa, A., Pullammanappallil, P., Ok, Y.S., Cao, X. 2016. A review of biochar as a low-cost adsorbent for aqueous heavy metal removal. Crit Rev Env Sci Tec. 46, 406-433.

[11] Kołodyńska, D., Krukowska, J., Thomas, P. 2017. Comparison of sorption and desorption studies of heavy metal ions from biochar and commercial active carbon. Chem. Eng. J. 307, 353-363.

[12] Liu, T., Wei, D., Zhang, G., Hu, L., Du, B., Wei, Q. 2016. A comparison of the influence of flocculent and granular structure of sludge on activated carbon: preparation, characterization and application. Rsc Adv. 6, 87353-87361.

[13] Ming, H., Zhang, S., Pan, B., Zhang, W., Lu, L., Zhang, Q. 2012. Heavy metal removal from water/wastewater by nanosized metal oxides: A review. J Hazard Mater. 211-212, 317-331.

[14] Noda, I., Ozaki, Y. 2005. Two-dimensional correlation spectroscopy: applications in vibrational and optical spectroscopy. John Wiley & Sons.

[15] Pellera, F.M., Giannis, A., Kalderis, D., Anastasiadou, K., Stegmann, R., Wang, J.Y., Gidarakos, E. 2012. Adsorption of Cu(II) ions from aqueous solutions on biochars prepared from agricultural by-products. J Environ Manage. 96, 35-42.

[16] Phong, D.D., Hur, J. 2016. Non-catalytic and catalytic degradation of effluent dissolved organic matter under UVA-and UVC-irradiation tracked by advanced spectroscopic tools. Water Res. 105, 199-208

[17] Qian, L., Zhang, W., Yan, J., Han, L., Gao, W., Liu, R., Chen, M. 2016. Effective removal of heavy metal by biochar colloids under different pyrolysis temperatures. Bioresour. Technol. 206, 217-224.

[18] Sheng, G., Li, J., Shao, D., Hu, J., Chen, C., Chen, Y., Wang, X. 2010. Adsorption of copper(II) on multiwalled carbon nanotubes in the absence and presence of humic or fulvic acids. J Hazard Mater. 178, 333-340.

[19] Sun, W.L., Xia, J., Li, S., Sun, F. 2012. Effect of natural organic matter (NOM) on Cu(II) adsorption by multi-walled carbon nanotubes: Relationship with NOM properties. Chem. Eng. J. 200-202, 627-636.

[20] Sun, X.F., Wang, S.G., Zhang, X.M., Chen, J.P., Li, X.M., Gao, B.Y., Ma, Y. 2009. Spectroscopic study of Zn^{2+} and Co^{2+} binding to extracellular polymeric substances (EPS) from aerobic granules. J. Colloid Interface Sci. 335, 11-17.

[21] Tavakoli, O., Goodarzi, V., Saeb, M. R., Mahmoodi, N. M., Borja, R. 2017. Competitive removal of heavy metal ions from squid oil under isothermal condition by CR11 chelate ion exchanger. J Hazard Mater. 334, 256-266.

[22] Tay, J., Chen, X., Jeyaseelan, S., Graham, N. 2001. A comparative study of anaerobically digested and undigested sewage sludges in preparation of activated carbons. Chemosphere. 44, 53-57.

[23] Tian, X., Li, T., Yang, K., Xu, Y., Lu, H., Lin, D. 2012. Effect of humic acids on physicochemical property and Cd(II) sorption of multiwalled carbon nanotubes. Chemosphere. 89, 1316-1322.

[24] Tong, X.J., Li, J.Y., Yuan, J.H., Xu, R.K. 2011. Adsorption of Cu(II) by biochars generated from three crop straws. Chem. Eng. J. 172, 828-834.

[25] Vigneswaran, S. 2006. Effluent organic matter (EfOM) in wastewater: constituents, effects, and treatment. Crit Rev Env Sci Tec. 36, 327-374.

[26] Wang, J., Chen, C. 2009. Biosorbents for heavy metals removal and their future. Biotechnol. Adv. 27, 195-226.

[27] Wei, D., Dong, H., Wu, N., Ngo, H.H., Guo, W., Du, B., Wei, Q. 2016a. A fluorescence approach to assess the production of soluble microbial products from aerobic granular sludge under the stress of 2,4-Dichlorophenol. Sci Rep. 6, 24444.

[28] Wei, D., Li, M., Wang, X., Han, F., Li, L., Guo, J., Ai, L., Fang, L., Liu, L., Du, B. 2016b. Extracellular polymeric substances for Zn (II) binding during its sorption process onto aerobic granular sludge. J Hazard Mater. 301, 407-415.

[29] Wei, D., Ngo, H.H., Guo, W., Xu, W., Zhang, Y., Du, B., Wei, Q. 2016c. Biosorption of effluent organic matter onto magnetic biochar composite: Behavior of fluorescent components and

their binding properties. Bioresour Technol. 214, 259-265.

[30] Wei, D., Shi, L., Zhang, G., Wang, Y., Shi, S., Wei, Q., Du, B. 2014. Comparison of nitrous oxide emissions in partial nitrifying and full nitrifying granular sludge reactors treating ammonium-rich wastewater. Bioresour Technol. 171, 487-490.

[31] Xu, H., Pan, J., Zhang, H., Yang, L. 2016. Interactions of metal oxide nanoparticles with extracellular polymeric substances (EPS) of algal aggregates in an eutrophic ecosystem. Ecol. Eng. 94, 464-470.

[32] Yang, J., Zhang, X., Sun, Y., Li, A., Ma, F. 2017. Formation of soluble microbial products and their contribution as electron donors for denitrification. Chem. Eng. J. 326, 1159-1165.

[33] Yang, K., Xing, B. 2009. Sorption of Phenanthrene by Humic Acid-Coated Nanosized TiO_2 and ZnO. Environ. Sci. Technol. 43, 1845-51.

[34] Yang, S., Li, L., Pei, Z., Li, C., Shan, X.Q., Wen, B., Zhang, S., Zheng, L., Zhang, J., Xie, Y. 2014. Effects of humic acid on copper adsorption onto few-layer reduced graphene oxide and few-layer graphene oxide. Carbon. 75, 227-235.

[35] Yu, G.H., Wu, M.J., Wei, G.R., Luo, Y.H., Ran, W., Wang, B.R., Zhang, J.C., Shen, Q.R. 2012a. Binding of organic ligands with Al(III) in dissolved organic matter from soil: implications for soil organic carbon storage. Environ. Sci. Technol. 46, 6102-6109.

[36] Yu, J., Lv, L., Lan, P., Zhang, S., Pan, B., Zhang, W. 2012b. Effect of effluent organic matter on the adsorption of perfluorinated compounds onto activated carbon. J Hazard Mater. 225-226, 99-106.

Figure captains

Fig.1 Pseudo-first-order kinetics (A) and Pseudo-second-order kinetics (B) fit of Cu(II) sorption onto AGS-BC in the absence and presence of EfOM.

Fig. 2 Langmuir and Freundlich adsorption isotherms fit of Cu(II) sorption onto AGS-BC in the presence and absence of EfOM.

Fig. 3 Changes in 3D-EEM spectra of EfOM samples from batch biosorption processes: (A) raw EfOM; (B) raw EfOM in the presence of 10 mg/L Cu(II); (C) raw EfOM in the presence of 20 mg AGS-BC; (D) raw EfOM in the presence of 20 mg AGS-BC and 10 mg/L Cu(II).

Fig. 4 FRI distribution of EfOM samples during the biosorption process: (A) raw EfOM; (B) EfOM + Cu(II); (C) EfOM+AGS-BC; (D) EfOM+AGS-BC+Cu(II).

Fig. 5 Synchronous fluorescence spectra of interaction between EfOM and Cu(II).

Fig. 6 Synchronous map (A) and asynchronous map (B) 2D correlation maps generated from the synchronous fluorescence spectra.

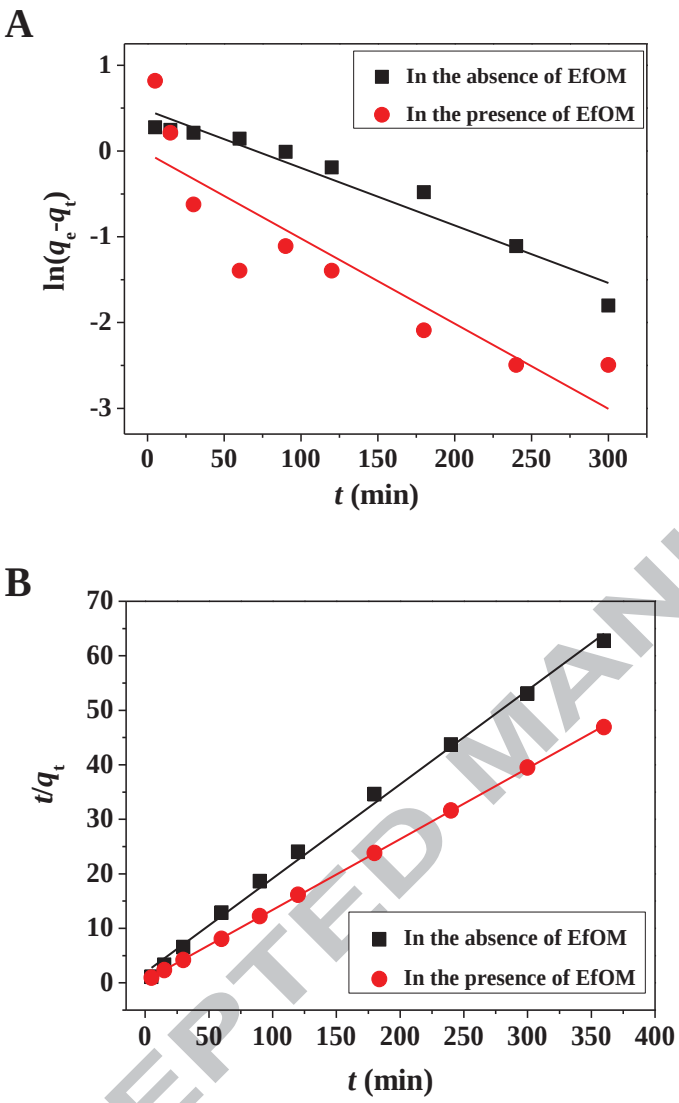

Fig.1 Pseudo-first-order kinetics (A) and Pseudo-second-order kinetics (B) fit of Cu(II) sorption onto AGS-BC in the absence and presence of EfOM.

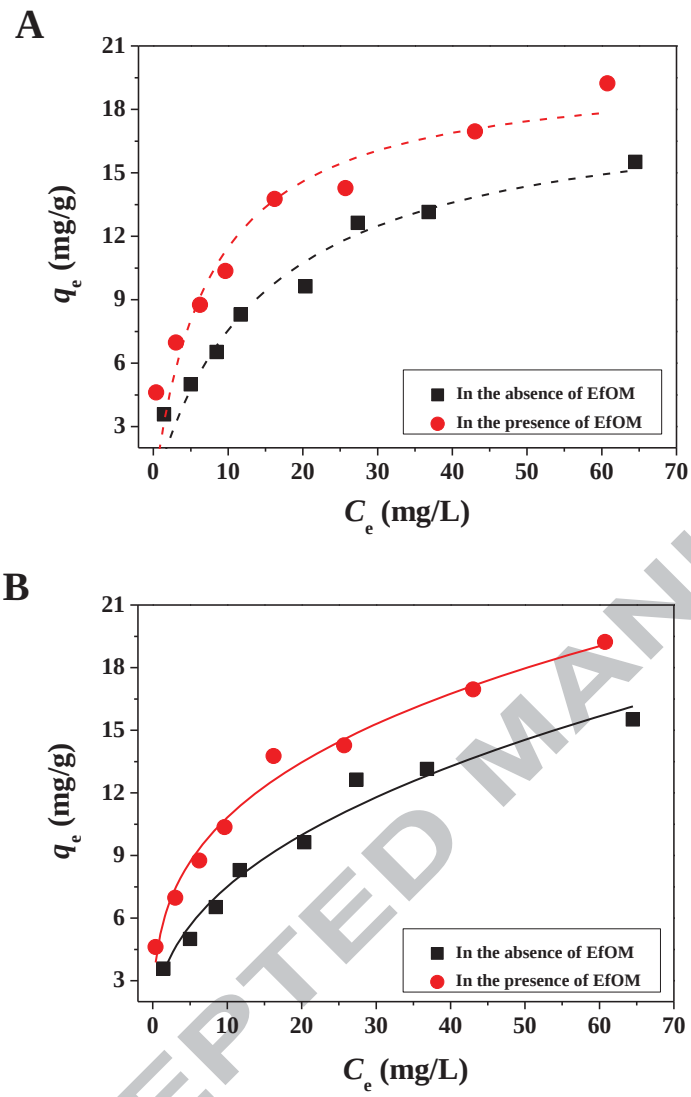

Fig. 2 Langmuir and Freundlich adsorption isotherms fit of Cu(II) sorption onto AGS-BC in the presence and absence of EfOM.

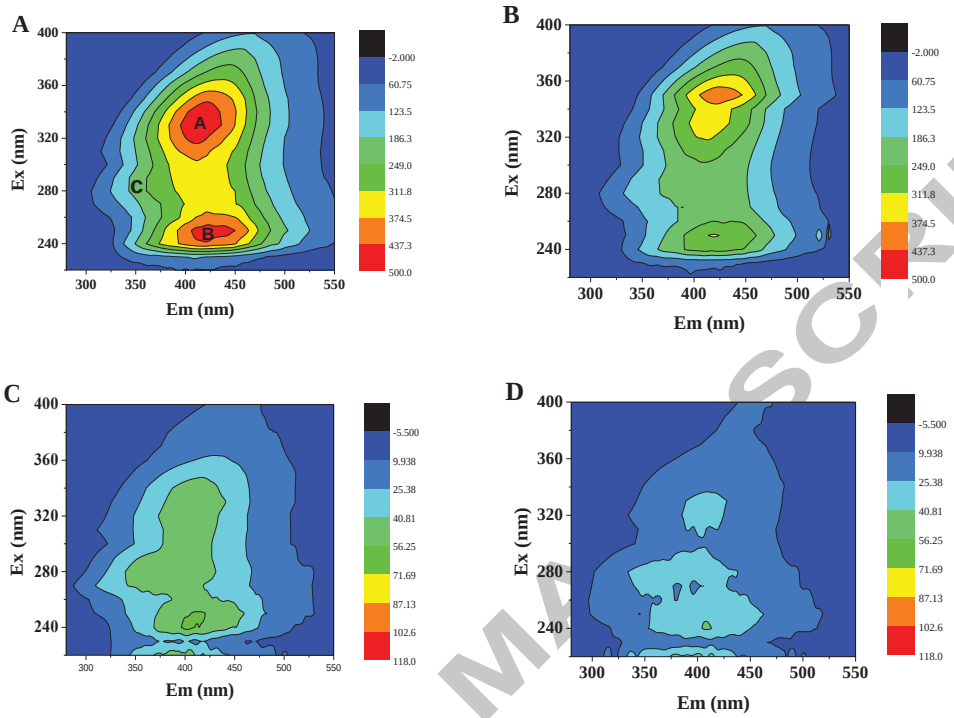

Fig. 3 Changes in 3D-EEM spectra of EfOM samples from batch biosorption processes: (A) raw EfOM; (B) raw EfOM in the presence of 10 mg/L Cu(II); (C) raw EfOM in the presence of 20 mg AGS-BC; (D) raw EfOM in the presence of 20 mg AGS-BC and 10 mg/L Cu(II).

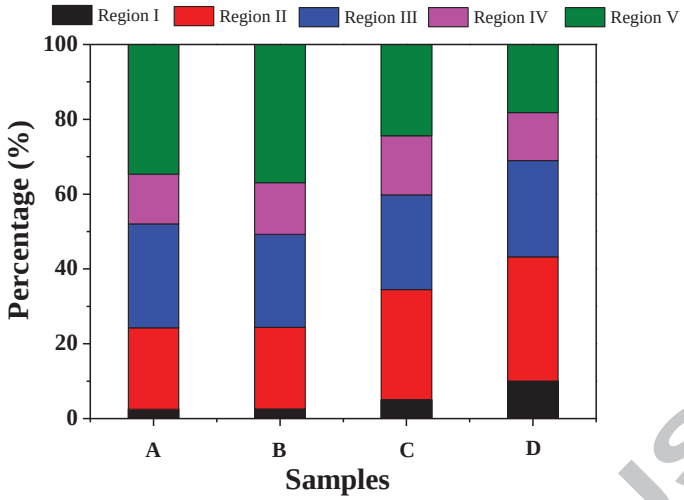

Fig. 4 FRI distribution of EfOM samples during the biosorption process: (A) raw EfOM; (B) EfOM + Cu(II); (C) EfOM+AGS-BC; (D) EfOM+AGS-BC+Cu(II).

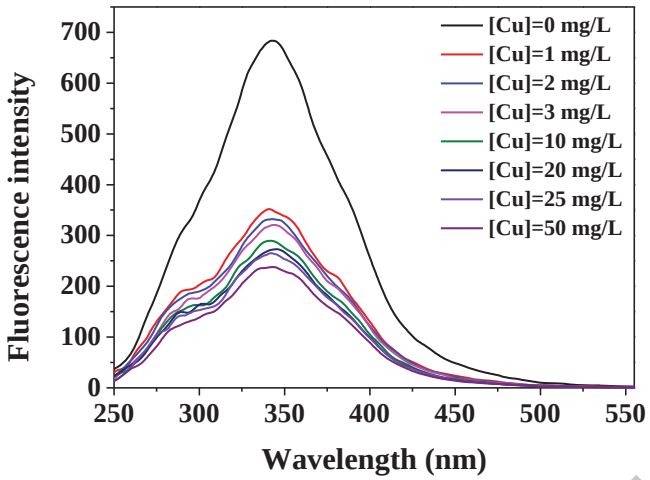

Fig. 5 Synchronous fluorescence spectra of interaction between EfOM and Cu(II).

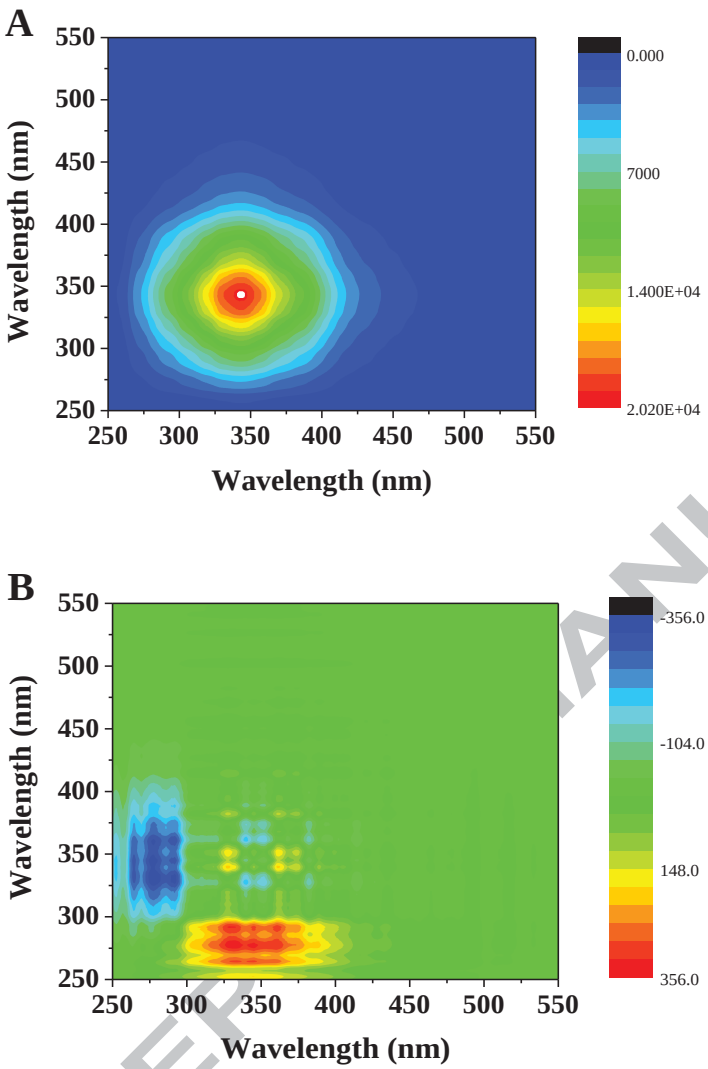

Fig. 6 Synchronous map (A) and asynchronous map (B) 2D correlation maps generated from the synchronous fluorescence spectra.

Table 1 Constants and correlation coefficients for the two kinds of kinetic models.

Model	Parameter	AGS-BC without EfOM	AGS-BC with EfOM
Pseudo-First Order Model	q_e (mg/g)	1.604	0.9725
	k_1 (min^{-1})	0.0067	0.00993
	R^2	0.9393	0.7794
Pseudo-Second Order Model	q_e (mg/g)	5.790	7.699
	k_2 (mg/(g·min))	0.01584	0.04261
	R^2	0.9965	0.9999

Table 2 Constants and correlation coefficients of adsorption isotherms for the sorption of Cu(II) onto AGS-BC with and without EfOM.

Model	Parameter	AGS-BC without EfOM	AGS-BC with EfOM
Langmuir equation	q_m (mg/g)	18.52	20.04
	B (L/mg)	0.06893	0.1340
	R^2	0.9464	0.8749
Freundlich equation	K_f	2.919	5.238
	$1/n$	0.4105	0.3151
	R^2	0.9711	0.9827

Graphical abstract